2019

Change Detection Using Landsat and Worldview Images

Chiman Kwan

Bryan Chou

Leif Hagen

Daniel Perez
Old Dominion University

Yuzhong Shen
Old Dominion University, yshen@odu.edu

See next page for additional authors

Original Publication Citation

Kwan, C., Chou, B., Hagen, L., Perez, D., Shen, Y., Li, J., & Koperski, K. (2019). *Change detection using Landsat and Worldview images.* Paper presented at the Algorithms, Technologies, and Applications for Multispectral and Hyperspectral Imagery XXV, 16-18 April 2019, Baltimore, Maryland, April 14-18, 2019.

Change Detection Using Landsat and Worldview Images

Chiman Kwan*[a], Bryan Chou[a], Leif Hagen[a], Daniel Perez[b], Yuzhong Shen[b], Jiang Li[b], and Krzysztof Koperski[c]

[a]Applied Research LLC, 9605 Medical Center Dr., Rockville, MD, 20850, USA; [b]Old Dominion University, Norfolk, VA, 23529, USA; [c]Digital Globe Inc., 1300 W. 120th Ave., Westminster, CO 80234, USA.

ABSTRACT

This paper presents some preliminary results using Landsat and Worldview images for change detection. The studied area had some significant changes such as construction of buildings between May 2014 and October 2015. We investigated several simple, practical, and effective approaches to change detection. For Landsat images, we first performed pansharpening to enhance the resolution to 15 meters. We then performed a chronochrome covariance equalization between two images. The residual between the two equalized images was then analyzed using several simple algorithms such as direct subtraction and global Reed-Xiaoli (GRX) detector. Experimental results using actual Landsat images clearly demonstrated that the proposed methods are effective. For Worldview images, we used pansharpened images with only four bands for change detection. The performance of the aforementioned algorithms is comparable to that of a commercial package developed by Digital Globe.

Keywords: Change detection, Landsat, Worldview, pansharpening, GRX, chronochrome

1. INTRODUCTION

Change detection using medium resolution Landsat images and high resolution Worldview images has many important applications such as fire damage assessment, flood damage assessment, etc. Landsat images are complementary to Worldview in that Landsat has regular 16-day revisits whereas Worldview images have infrequent and irregular collections. More importantly, Landsat can detect relatively large changes and Worldview images can allow very detailed classification of changes.

In the past decades, there have been many papers discussing change detection[1-2] using multispectral (MS)[3-9] and hyperspectral (HS)[10-17] images. Some algorithms first perform covariance equalization and then perform some residual analysis using anomaly detection methods[18-22]. One critical issue is the registration between the pair of images. In Eismann's book[13], it was mentioned that covariance equalization (CE)[14] is more robust to registration errors and chronochrome (CC)[23] is more accurate in change detection if registration accuracy is sub-pixel.

In this paper, we investigated several simple, practical, and effective approaches to change detection. For Landsat images, we first performed pansharpening to enhance the resolution to 15 meters. We then performed a chronochrome covariance equalization between two images. The residual was then analyzed using several simple algorithms such as direct subtraction and global Reed-Xiaoli (GRX) detector[25]. For Worldview images, we used pansharpened images with only 4 bands. The performance of the aforementioned change detection algorithms is comparable to that of a commercial package known as Geospatial Big Data Platform (GBDX) developed by Digital Globe. Experimental results using actual Landsat and Worldview images clearly demonstrated that those simple methods are effective.

Our paper is organized as follows. Section 2 briefly reviews the methods, including pansharpening, prediction using chronochrome, and residual analysis, used in change detection. Section 3 presents change detection results using Landsat images. Section 4 includes change detection results using Worldview images. Finally, concluding remarks are provided in Section 5.

* Address all correspondence to: Chiman Kwan, chiman.kwan@signalpro.net

2. METHODS

For change detection using Landsat and Worldview images, the algorithms used in both cases are similar.

2.1 Pansharpening using GSA

The original Landsat 8 images retrieved from the USGS data archive have 30 m resolution except the pan band. In order to improve the resolution for better change detection, we applied a pansharpening algorithm to improve the resolution to 15 m. The Gram-Schmidt Adaptive (GSA)[27-28] was adopted in our study for its simplicity and effectiveness.

For Worldview images, we were given high resolution pansharpened images from Digital Globe.

2.2 Change Detection

Change detection involves two images. Figure 1 shows a simplified view of change detection, which has two parts[25]:

1) *Prediction/Transformation*. Transform the original reference image (**R**) and testing image (**T**) to new space as **PR** and **PT**.
2) *Change Evaluation*. Evaluate the difference between the transformed image pair and output a single band detection image.

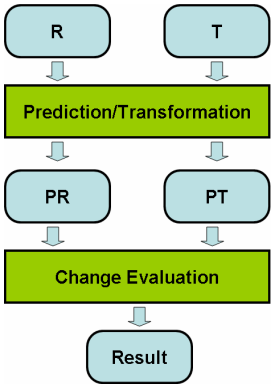

Figure 1. Illustration of change detection between two images. R and T denote reference and test images, respectively.

Prediction using chronochrome (CC)

The procedures of CC are as follows:

1. Compute mean and covariance of R and T as m_R, C_R, m_T, C_T
2. Compute cross-covariance between R and T as C_{TR}
3. Do transformation.

$$PR(i) = C_{TR}C_R^{-1}\left(R(i) - m_R\right) + m_T, \quad PT = T \tag{1}$$

Change Evaluation

Direct Subtraction Using near infrared (NIR) band only: After the preprocessing occurs, the NIR mask is generated simply by calculating the per-pixel difference between the two images of the NIR band. The greater the difference between the two, the higher the index the NIR mask will have.

Similarity Angle Mapper (SAM)[24]: The similarity measure, SAM, between the two radiance profiles, $\mathbf{s}_i$ and $\mathbf{r}_j$, SAM($\mathbf{s}_i, \mathbf{r}_j$) is then computed as:

$$SAM(\mathbf{s}_i, \mathbf{r}_j) = \cos^{-1}\left(\frac{\langle \mathbf{s}_i, \mathbf{r}_j \rangle}{\|\mathbf{s}_i\| \|\mathbf{r}_j\|}\right) \tag{2}$$

where $\left\langle \mathbf{s}_i, \mathbf{r}_j \right\rangle = \sum_{l=1}^{L} s_{iL} r_{jL}$ and $\left\| \mathbf{s}_i \right\| = \left(\sum_{l=1}^{L} {s_{iL}}^2 \right)^{1/2}$ and $\left\| \mathbf{r}_j \right\| = \left(\sum_{l=1}^{L} {r_{jL}}^2 \right)^{1/2}$.

Global Reed-Xiaoli (GRX) detector: Here we briefly describe the GRX detector. Given two images (Reference and Test), we first performance a covariance equalization to histogram match the Test image to the Reference image. After that, we apply a Reed-Xiaoli (RX)[25] algorithm for each pixel vector x. The RX detector is given by

$$D(x) = x^T R^{-1} x \tag{3}$$

where R is the covariance of the background. A large value of $D(x)$ indicates that there is a high probability that x is different from its background.

These individual masks are then thresholded along their grayscale values to produce a binary image where a success indicates a change at that location between the images.

3. CHANGE DETECTION USING LANDSAT IMAGES

The goal of change detection is to accurately detect areas of change contained between a pair of two satellite images. As shown in Table 1, Landsat images are comprised eleven bands of information: coastal, RGB, NIR, SWIR 1-2, Panchromatic, Cirrus, and TIRS 1-2. Most bands in the Landsat images are of a resolution of 30 meters. Bands 10 and 11 have 100 m resolution but upsampled to 30 m. So, all bands have a resolution of 15 meters after pansharpening, resulting in an image size of 119x293 for the images we use. The algorithm uses the information contained within the bands at each pixel to determine whether or not there exists urban change between the pair of images at that location.

Table 1: Landsat bands

Bands	Wavelength(micrometers)	Resolution(meters)
Band 1 - Ultra Blue (coastal/aerosol)	0.435 - 0.451	30
Band 2 - Blue	0.452 - 0.512	30
Band 3 - Green	0.533 - 0.590	30
Band 4 - Red	0.636 - 0.673	30
Band 5 - Near Infrared (NIR)	0.851 - 0.879	30
Band 6 - Shortwave Infrared (SWIR) 1	1.566 - 1.651	30
Band 7 - Shortwave Infrared (SWIR) 2	2.107 - 2.294	30
Band 8 - Panchromatic	0.503 - 0.676	15
Band 9 - Cirrus	1.363 - 1.384	30
Band 10 - Thermal Infrared (TIRS) 1	10.60 - 11.19	100 (30)
Band 11 - Thermal Infrared (TIRS) 2	11.50 - 12.51	100 (30)

Here, we present two sets of change detection results with two different starting dates.

3.1 Reference date: 5/4/14

Example 1: May 4, 2014 and October 11, 2014

We retrieved Landsat-8 images between May 2014 and October 2015 for an area of interest[26]. Many image pairs do not show much changes. By manually screening through the images, we started to observe some significant changes in October 11th, 2014. Figure 2 shows the receiver operating characteristics (ROC) curves of three detection methods: direct subtraction using near infrared band (NIR), SAM, and GRX. We can see that the NIR mask (change map) in red appears to be the most effective at finding the change which we expect to see while avoiding the areas we do not expect change. The change maps shown in Figure 3 are generated by picking a threshold corresponding to false alarm rate of 1%, meaning that 1% of all space that could contain a false alarm does. We did not apply any post-filtering to the change maps. If we do, the false alarms will be reduced.

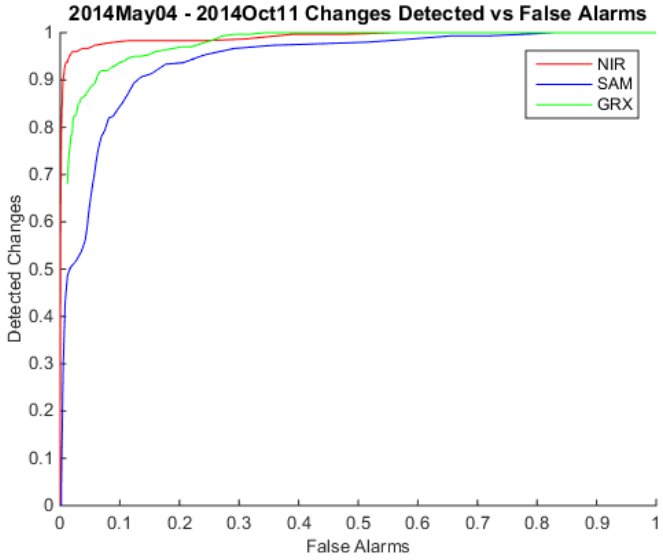

Figure 2. ROC Curves for changes between May 4, 2014 and Oct. 11, 2014.

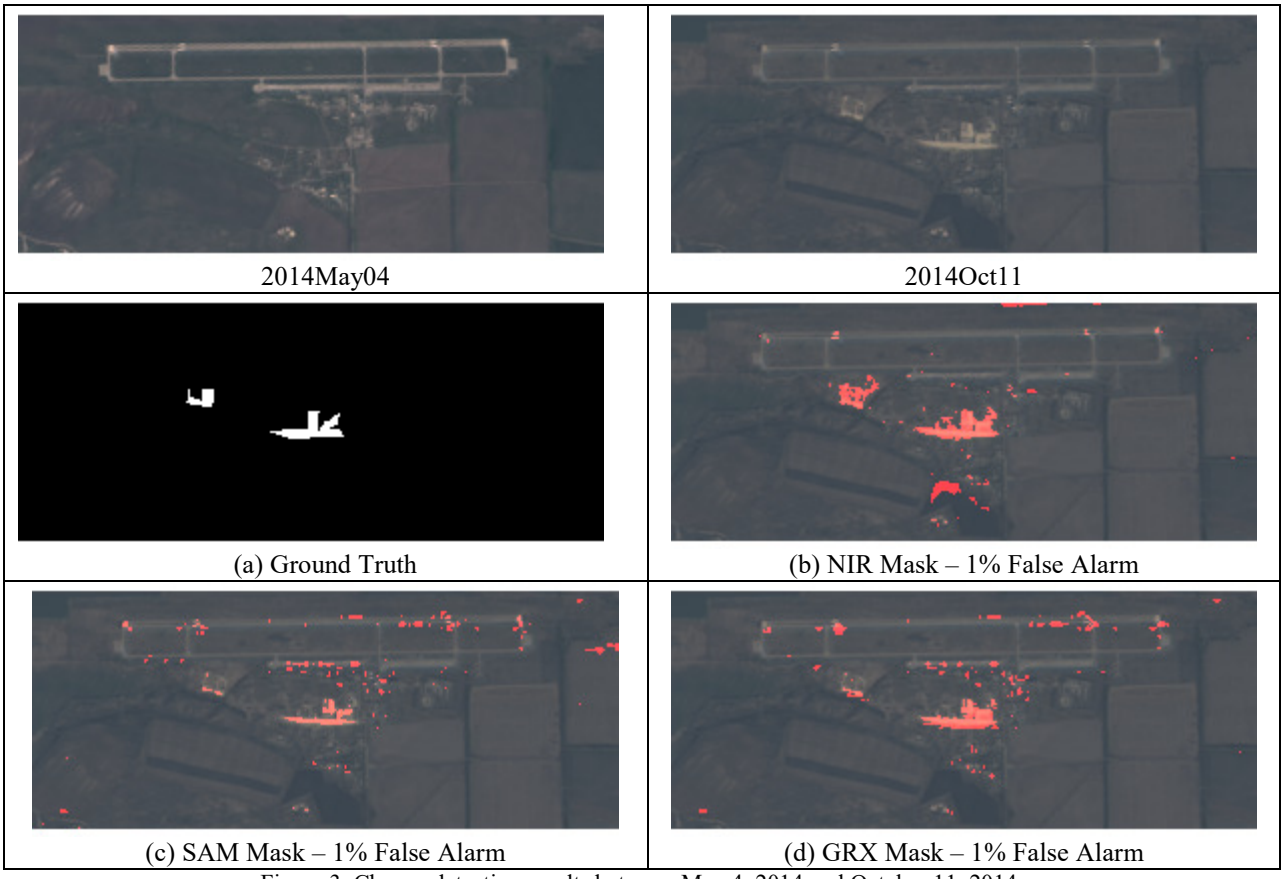

2014May04 | 2014Oct11

(a) Ground Truth | (b) NIR Mask – 1% False Alarm

(c) SAM Mask – 1% False Alarm | (d) GRX Mask – 1% False Alarm

Figure 3. Change detection results between May 4, 2014 and October 11, 2014.

Example 2: May 4, 2014 and March 21, 2015

Since the major changes in October 2014, there are some additional changes in the same area in March, 2015. The ROC curves in Figure 4 show the detection accuracy for the three methods. This time, the GRX method appears to have better performance than others. The change maps shown in Figure 5 corroborate the above observation.

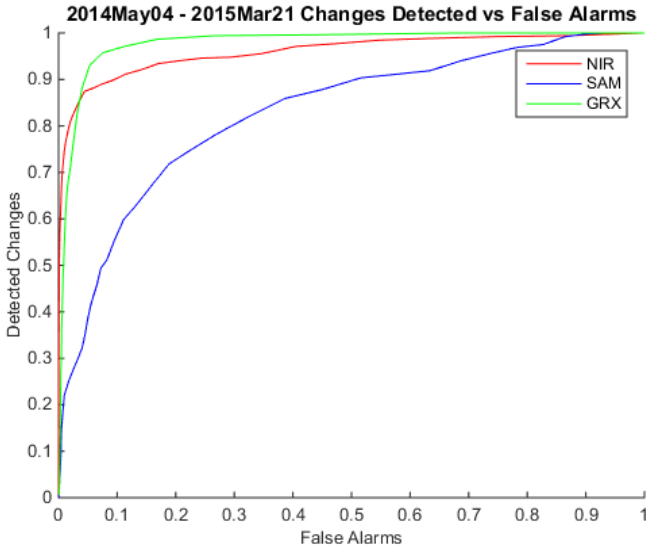

Figure 4. ROC Curves of three methods for changes between May 4, 2014 and March 21, 2015.

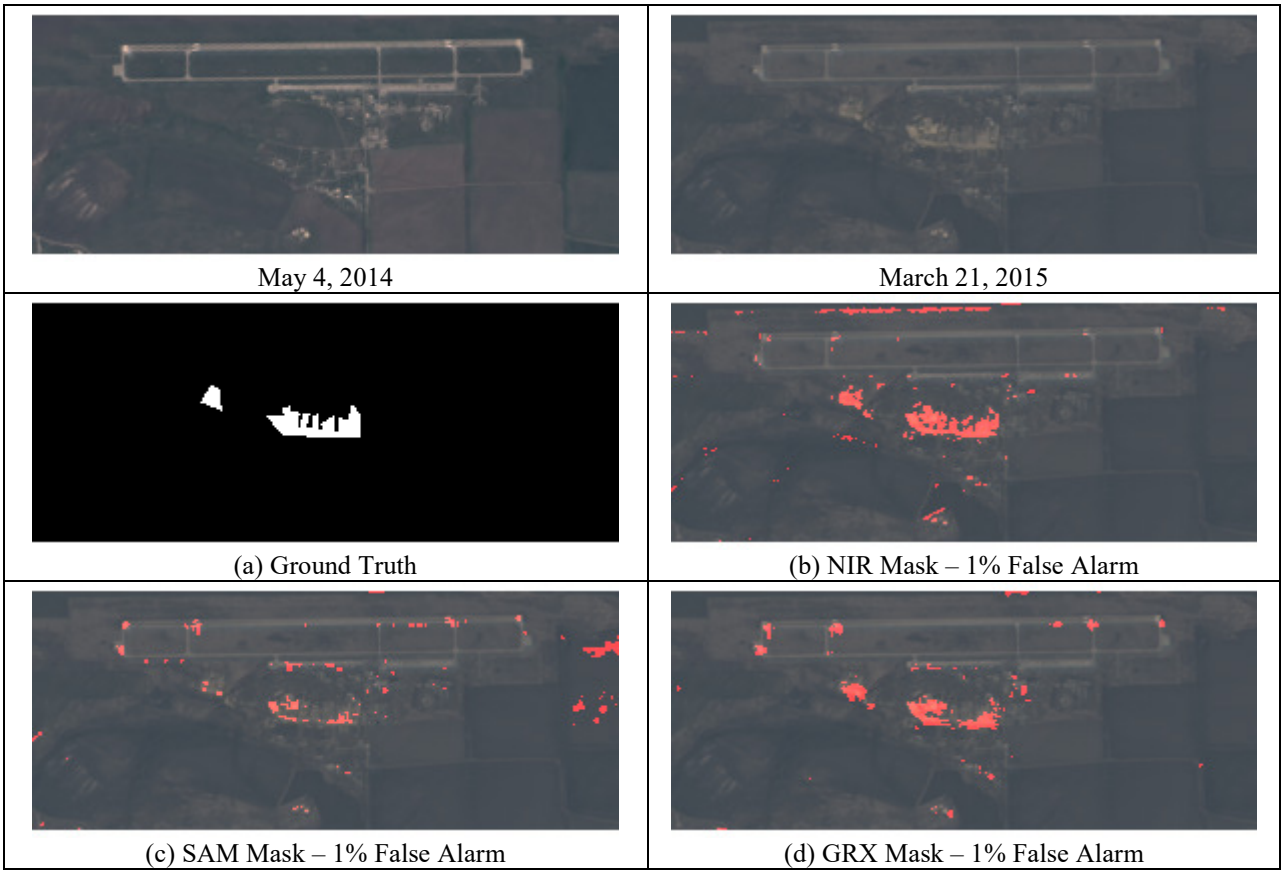

Figure 5. Change detection results between May 4, 2014 and March 21, 2015.

Example 3: May 4, 2014 and May 23, 2015

There appears to be some minor changes after March, 2015. Figure 6 shows the ROC curves of three methods between May 4, 2014 and May 23, 2015. It can be seen that direct subtraction using NIR is overwhelmingly better than others. From the change detection results shown in Figure 7, we can also observe the same trend.

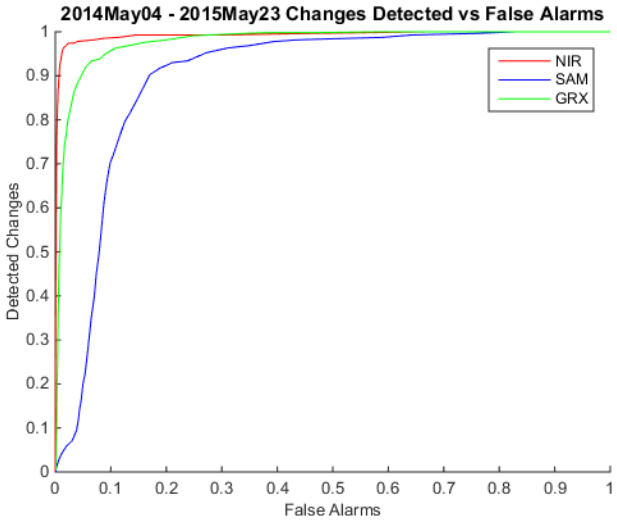

Figure 6. ROC Curves of three methods for changes between May 4, 2014 and May 23, 2015.

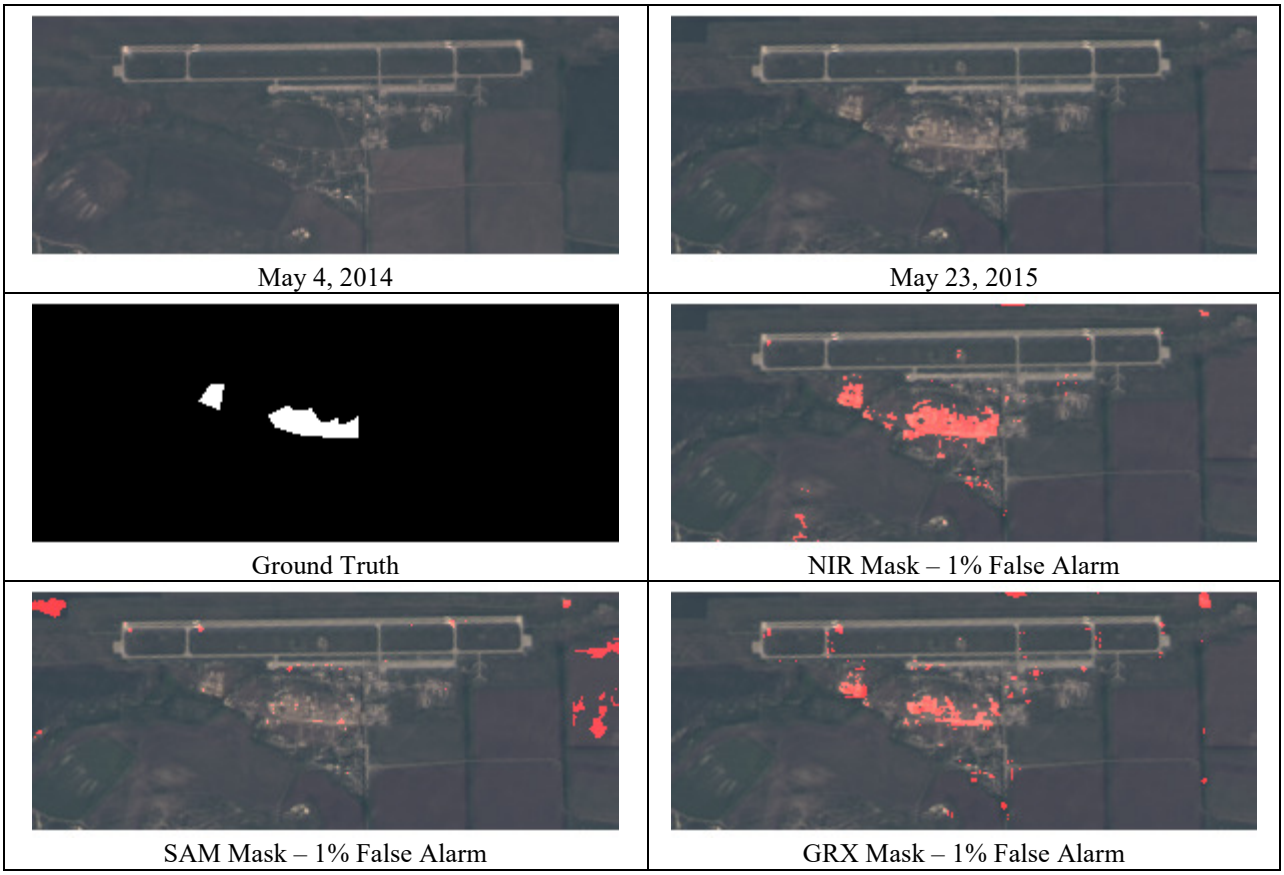

Figure 7. Change detection results between May 4, 2014 and May 23, 2015.

Example 4: May 4, 2014 and September 19, 2015

This example shows the same trend as the previous examples. From the ROC curves in Figure 8, we can see that NIR results are very good with high detection percentage and low false alarms. The change maps in Figure 9 confirm the ROC curves.

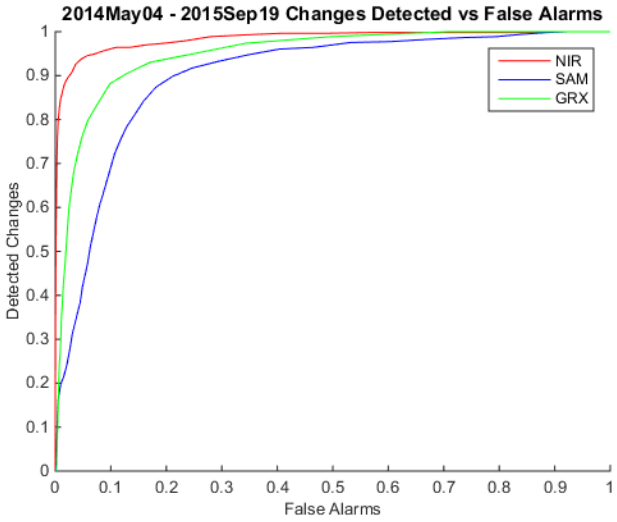

Figure 8. ROC Curves of three methods for changes between May 4, 2014 and September 19, 2015.

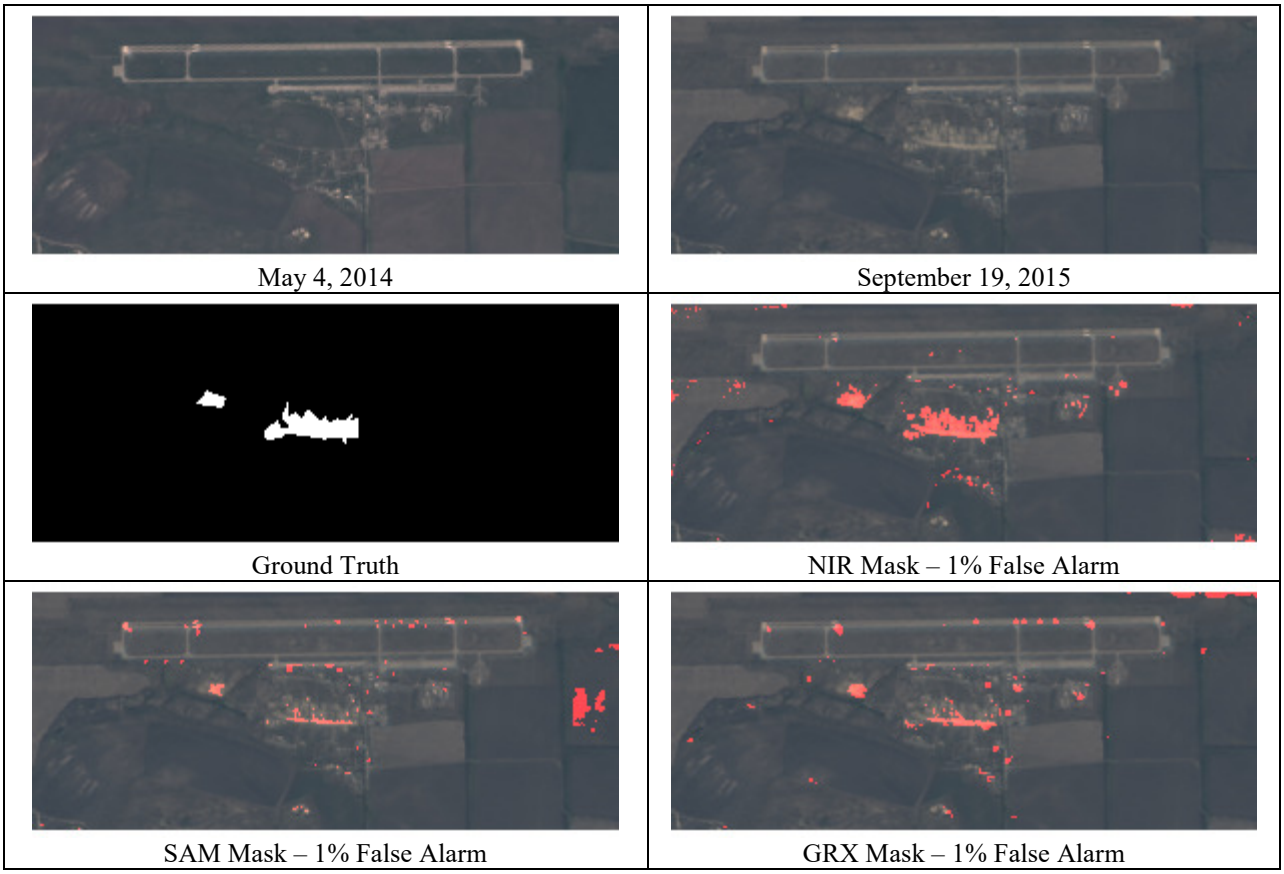

Figure 9. Change detection results between May 4, 2014 and September 19, 2015.

3.2 Reference October 11, 2014

We have additionally tested our method using a reference point (October 11, 2014) after much of the changes have already occurred. In these types of tests, we expect to see a much more loosely defined map, as changes between the two images are likely to be less apparent and vibrant than in the previous sets of images. Because of this, we would expect to see a higher quantity of false alarms, as the algorithm attempts to normalize the data it gathers from the masks, since those false alarms would likely be more similar to the actual changes we expect than before (as they are in reality, as well).

Example 1: October 11, 2014 and May 23, 2015

From ROC curves in Figure 10, it can be seen that GRX performs better than others. The change maps shown in Figure 11 at 1% FAR corroborate this observation.

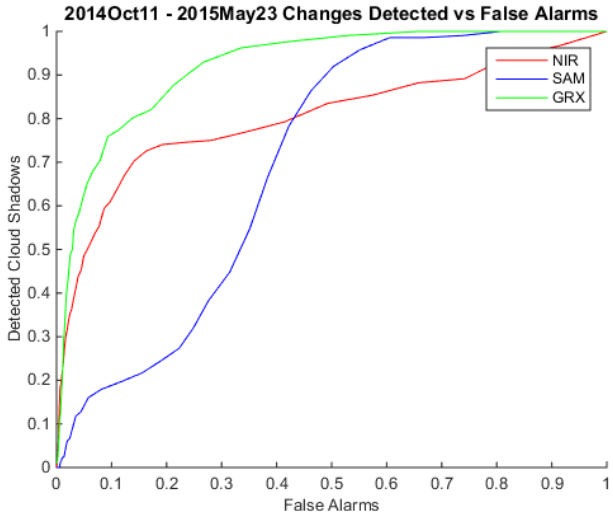

Figure 10. ROC Curves of three methods for changes between October 11, 2014 and May 23, 2015.

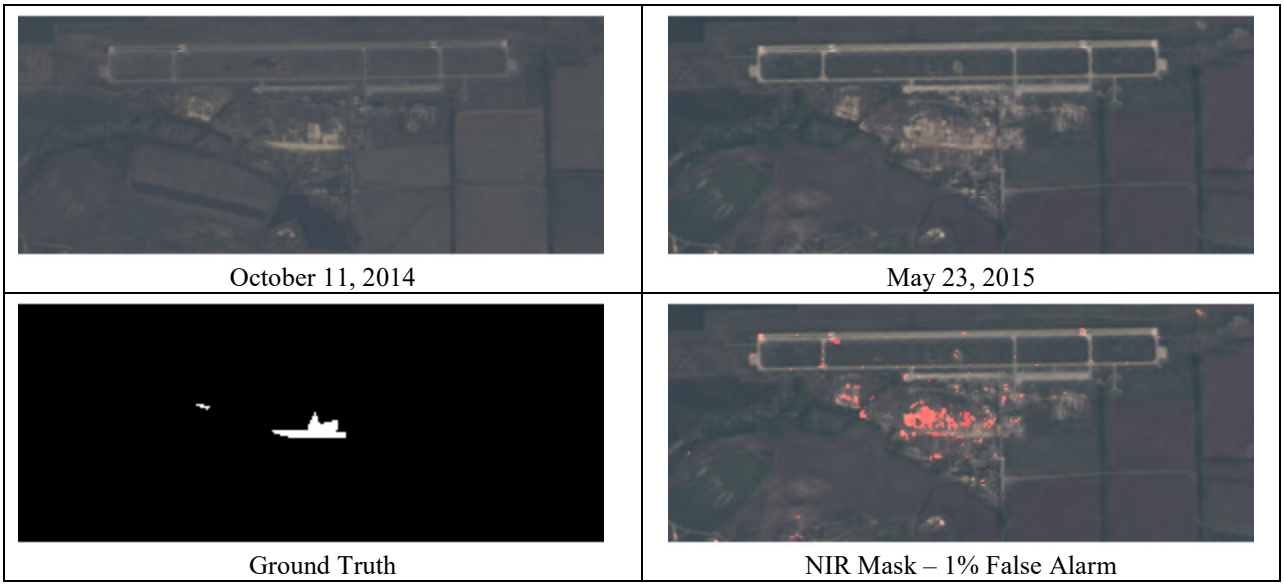

SAM Mask – 1% False Alarm

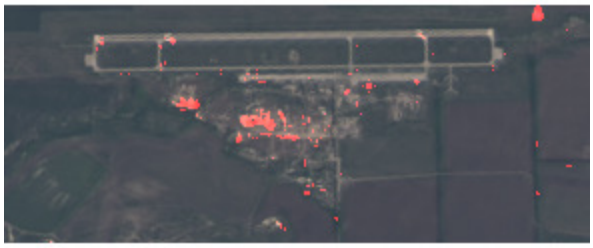

GRX Mask – 1% False Alarm

Figure 11. Change detection results at 1% false alarm rate between October 11, 2014 and May 23, 2015.

Example 2: Oct 11, 2014 and October 5, 2015

The ROC curves of three methods are shown in Figure 12 and the change maps are shown in Figure 13. In this example, GRX appears to perform better than others.

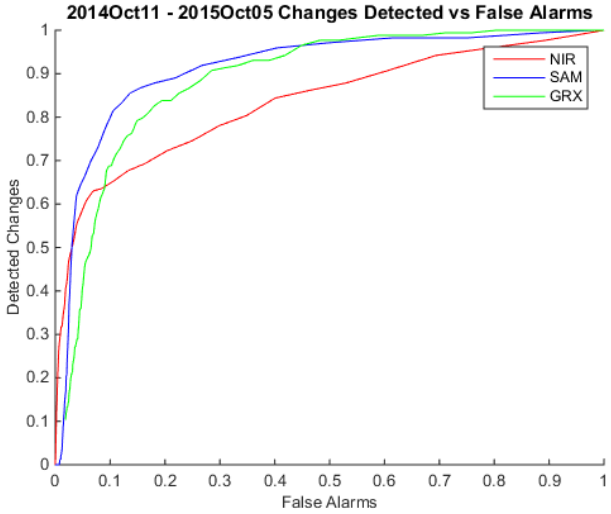

Figure 12. ROC Curves of three methods for changes between Oct 11, 2014 and October 5, 2015.

Oct 11, 2014

October 5, 2015

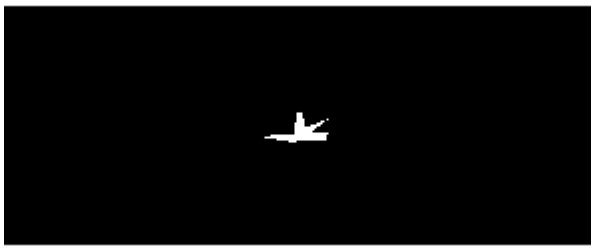

Ground Truth

NIR Mask – 1% False Alarm

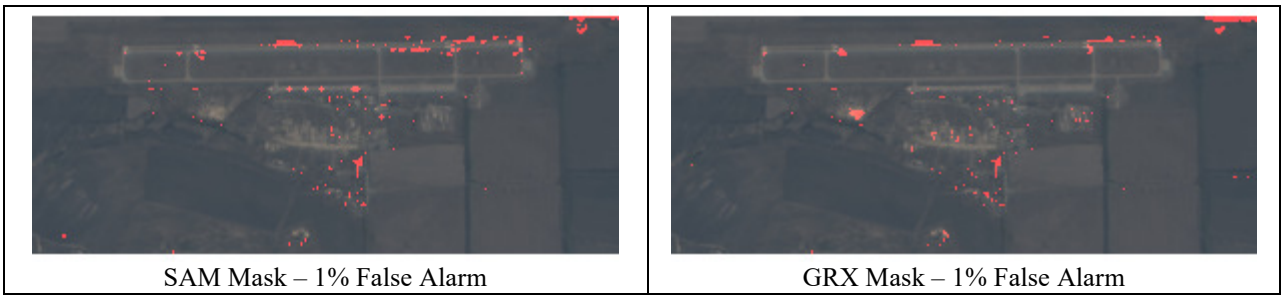

SAM Mask – 1% False Alarm | GRX Mask – 1% False Alarm

Figure 13. Change detection results at 1% false alarm rate between Oct 11, 2014 and October 5, 2015.

3.3 Discussions

Although there are more sophisticated change detection methods, we investigated three simple ones which are easy to implement. For change detection using Landsat images, we observe that the combination of CC and GRX methods yielded more consistent performance as compared to others. Other advanced methods will be tried in the future.

4. CHANGE DETECTION USING WORLDVIEW IMAGES

Here, we present three sets of change detection results using Worldview images.

Example 1: 04/24/2014 - 07/30/2015

Here, we retrieved Worldview images between May 2014 and October 2015. There are only a handful of images over that period. We now show change maps between 04/24/2014 - 07/30/2015. Four methods (NIR, SAM, GRX, and GBDX (Geospatial Big Data Platform)) were applied to generate the change maps. The change maps, except GBDX, shown in Figure 15 are generated by picking a threshold corresponding to false alarm rate of 3%, meaning that 3% of all space that could contain a false alarm does. From the ROC curves (Figure 14), GBDX has the best performance, followed by GRX. It should be noted that GBDX has only one point on the ROC curve because GBDX has a pre-determined fixed threshold to generate the change map.

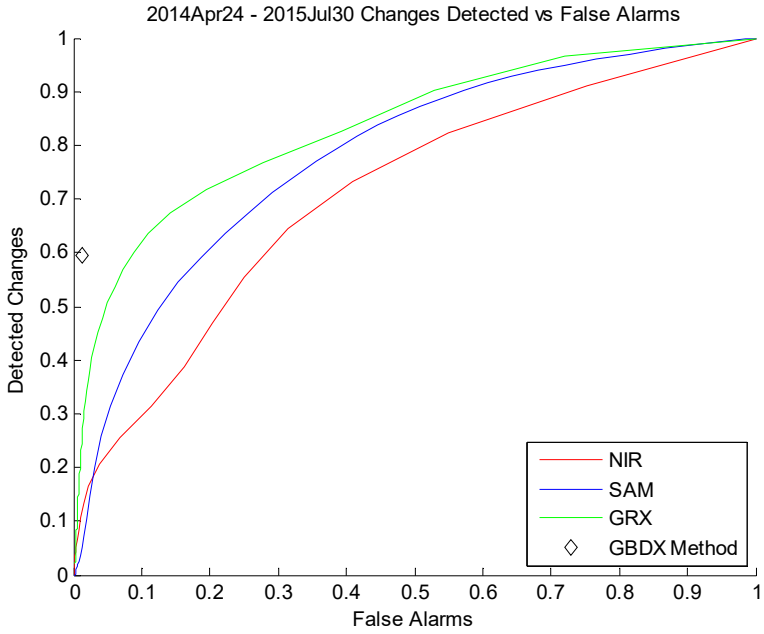

Figure 14. ROC Curves for changes between 04/24/2014 and 07/30/2015.

Original Image 04/24/2014

Original Image 07/30/2015

(a) Ground Truth

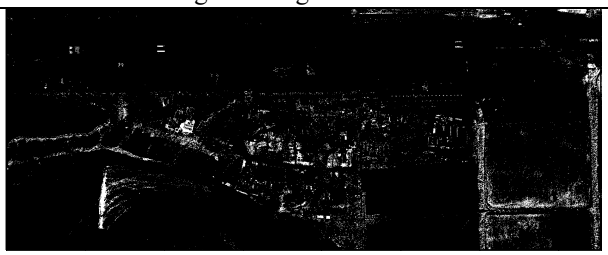

(b) NIR Mask – 3% False Alarm

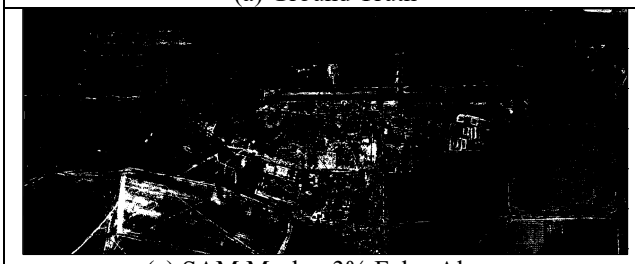

(c) SAM Mask – 3% False Alarm

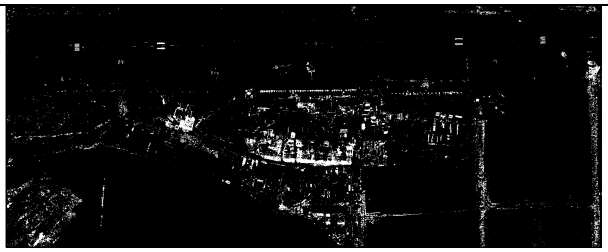

(d) GRX Mask – 3% False Alarm

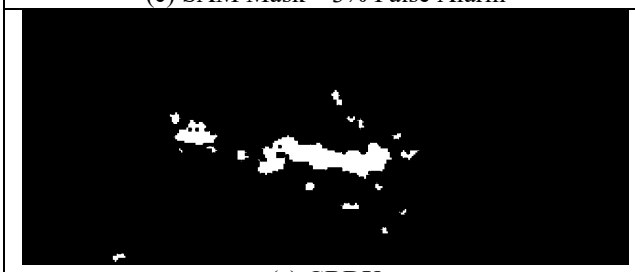

(e) GBDX

Figure 15. Change detection results between 04/24/2014 and 07/30/2015.

Example 2: 10/30/2014 - 05/28/2015

Since the major changes in October 2014, there are some additional changes in the same area in March, 2015. The ROC curves in Figure 16 show the detection accuracy for the four methods. This time, the GRX method appears to have better performance than others. As shown in Figure 17, GBDX has more clean change map because some post-filtering using morphological filters was used. In the other results, we did not apply any post-filtering.

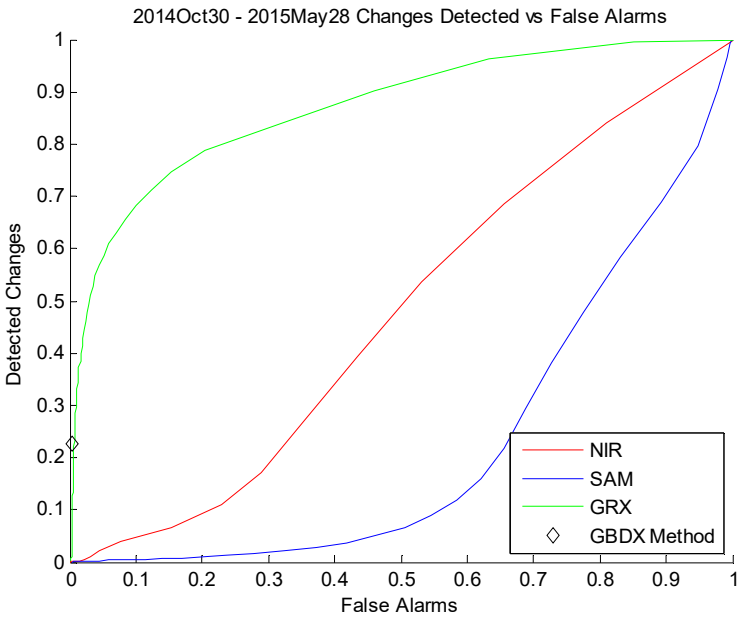

Figure 16. ROC Curves of three methods for changes between 10/30/2014 - 05/28/2015.

Original Image 10/30/2014

Original Image 05/28/2015

(a) Ground Truth

(b) NIR Mask – 3% False Alarm

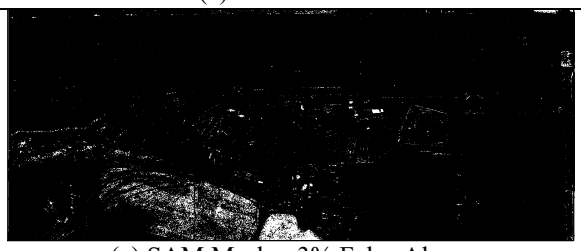

(c) SAM Mask – 3% False Alarm

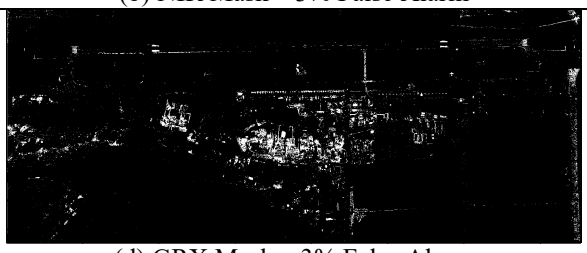

(d) GRX Mask – 3% False Alarm

GBDX

Figure 17. Change detection results between 10/30/2014 - 05/28/2015.

Example 3: 04/24/2014 - 10/30/2014

Figure 18 shows the ROC curves of four methods between April 24, 2014 and October 30, 2014. It can be seen that GBDX is overwhelmingly better than others. From the change detection results shown in Figure 19, we can also observe the same trend.

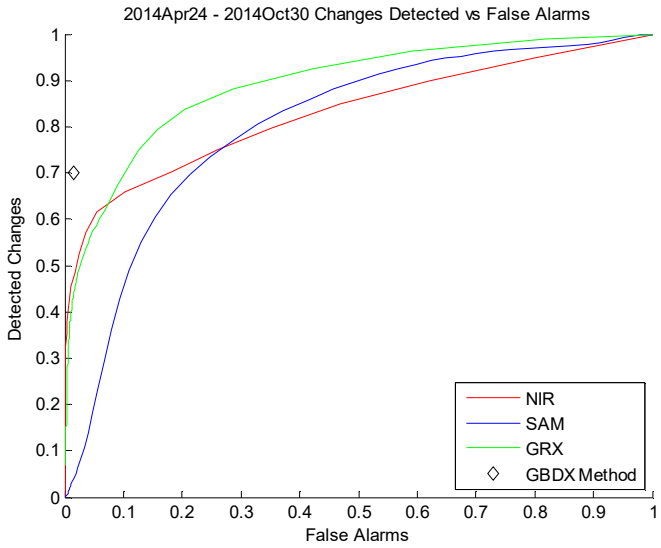

Figure 18. ROC Curves of three methods for changes between 04/24/2014 - 10/30/2014.

Original Image 04/24/2014

Original Image 10/30/2014

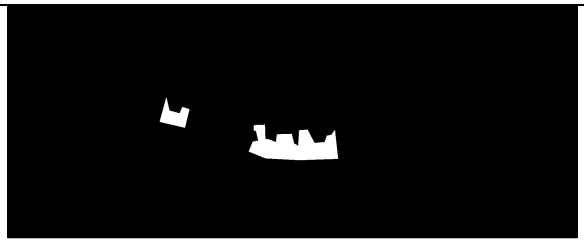

Ground Truth

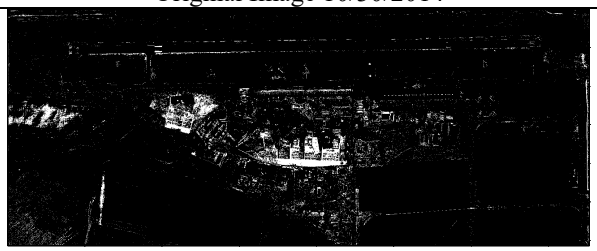

NIR Mask – 3% False Alarm

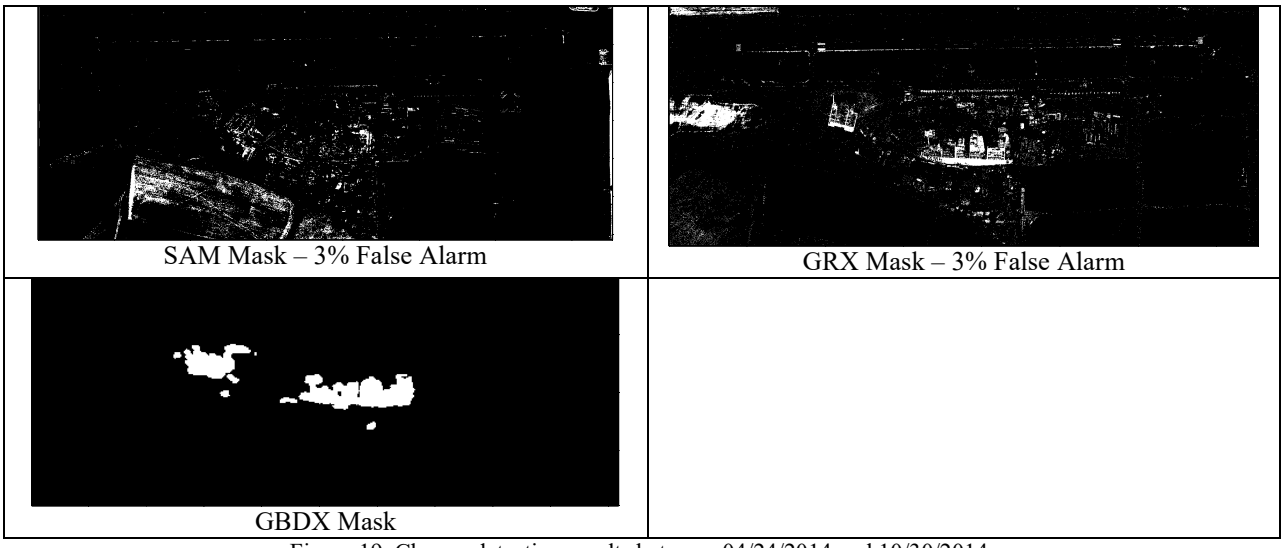

Figure 19. Change detection results between 04/24/2014 and 10/30/2014.

5. CONCLUSIONS

Here, we present some preliminary results of change detection using medium resolution images (Landsat) and high resolution images (Worldview). The aim is to see if we can use Landsat to detect some early signs of changes. If some early changes are detected, we can then collect high resolution images of the same area and perform more detailed change analysis. For Landsat images, we observed that GRX worked quite well. For Worldview images, the default change detection algorithms in GBDX was the best.

One future direction is to investigate more sophisticated algorithms such as deep learning for change detection.

ACKNOWLEDGEMENT

This research was supported by DARPA under contract #140D6318C0043. The views, opinions and/or findings expressed are those of the author and should not be interpreted as representing the official views or policies of the Department of Defense or the U.S. Government.

REFERENCES

[1] Radke, R.J., Andra, S., Al-Kofani, O. and Roysam, B., "Image change detection algorithms: a systematic survey," IEEE Transactions on Image Processing 14(3), 294–307 (2005)

[2] Bovolo, F. and Bruzzone, L., "The time variable in data fusion: A change detection perspective," IEEE Geoscience and Remote Sensing Magazine 3(3), 8–26 (2015)

[3] Dao, M., Kwan, C., Ayhan, B. and Tran, T., "Burn Scar Detection Using Cloudy MODIS Images via Low-rank and Sparsity-based Models," IEEE Global Conference on Signal and Information Processing 177 – 181 (2016)

[4] Dao, M., Kwan, C., Koperski, K. and Marchisio, G., "A Joint Sparsity Approach to Tunnel Activity Monitoring Using High Resolution Satellite Images," IEEE Ubiquitous Computing, Electronics & Mobile Communication Conference, 322-328 (2017)

[5] Kwan, C. and Ayhan, B., "Automatic target recognition system with online machine learning capability," Patent # 9940520, (2018)

[6] Perez, D., Banerjee, D., Kwan, C., Dao, M., Shen, Y., Koperski, K., Marchisio, G., and Li, J., "Deep Learning for Effective Detection of Excavated Soil Related to Illegal Tunnel Activities," IEEE Ubiquitous Computing, Electronics & Mobile Communication Conference 626-632, (2017)

[7] Lu, Y., Perez, D., Dao, M., Kwan, C. and Li, J., "Deep Learning with Synthetic Hyperspectral Images for Improved Soil Detection in Multispectral Imagery," IEEE Ubiquitous Computing, Electronics & Mobile Communication Conference (2018)
[8] Ayhan, B., Dao, M., Kwan, C., Chen, H., Bell, J.F. and Kidd, R., "Novel Utilization of Image Registration Techniques to Process Mastcam Images in Mars Rover with Applications to Image Fusion, Pixel Clustering, and Anomaly Detection," IEEE Journal of Selected Topics in Applied Earth Observations and Remote Sensing 4553 – 4564 (2017)
[9] Perez, D., Lu, Y., Kwan, C., Shen, Y., Koperski, K. and Li, J., "Combining Satellite Images with Feature Indices for Improved Change Detection," IEEE Ubiquitous Computing, Electronics & Mobile Communication Conference, (2018)
[10] Zhou, J., Kwan, C. and Ayhan, B., "Improved Target Detection for Hyperspectral Images Using Hybrid In-Scene Calibration," J. Appl. Remote Sens. 11(3) (2017)
[11] Ayhan, B. and Kwan, C., "Application of Deep Belief Network to Land Classification Using Hyperspectral Images," 14th International Symposium on Neural Networks 269-276 (2017)
[12] Ayhan, B., Kwan, C. and Zhou, J., "A New Nonlinear Change Detection Approach Based on Band Ratioing," Proc. SPIE 10644, Algorithms and Technologies for Multispectral, Hyperspectral, and Ultraspectral Imagery XXIV, 1064410, (2018)
[13] Eismann, M. Hyperspectral Remote Sensing, SPIE Press Monograph Vol. PM210, 2012.
[14] Schaum, A., "Local Covariance Equalization of Hyperspectral Imagery: Advantages and Limitations for Target Detection," IEEE Aerospace Conference (2004)
[15] Zhou, J., Ayhan, B., Kwan, C. and Eismann, M., "New and Fast algorithms for Anomaly and Change Detection in Hyperspectral images," International Symposium on Spectral Sensing Research, Missouri, (2010)
[16] Eismann, M. T., Meola, J. and Hardie, R. C., "Hyperspectral change detection in the presence of diurnal and seasonal variations," IEEE T. Geosci. Remote Sens 46, 237–249 (2008)
[17] Zhou, J. and Kwan, C., "High Performance Change Detection in Hyperspectral Images Using Multiple References," SPIE Defense + Security Conference, (2018)
[18] Wang, W., Li, S., Qi, H., Ayhan, B., Kwan, C. and Vance, S., "Identify Anomaly Component by Sparsity and Low Rank," IEEE Workshop on Hyperspectral Image and Signal Processing: Evolution in Remote Sensor (WHISPERS), (2015)
[19] Chang, C.-I. Hyperspectral Imaging, Springer, 2003.
[20] Li, S., Wang, W., Qi, H., Ayhan, B., Kwan, C. and Vance, S., "Low-rank Tensor Decomposition based Anomaly Detection for Hyperspectral Imagery," IEEE International Conference on Image Processing (ICIP), 4525 – 4529 (2015)
[21] Qu, Y., Guo, R., Wang, W., Qi, H., Ayhan, B., Kwan, C. and Vance, S., "Anomaly Detection in Hyperspectral Images Through Spectral Unmixing and Low Rank Decomposition," IEEE International Geoscience and Remote Sensing Symposium (IGARSS), 1855 – 1858 (2016)
[22] Qu, Y., Qi, H., Ayhan, B., Kwan, C. and Kidd, R., "Does Multispectral/Hyperspectral Pansharpening Improve the Performance of Anomaly Detection?" IEEE International Geoscience and Remote Sensing Symposium (IGARSS), 6130-6133 (2017)
[23] Schaum, A. and Stocker, A., "Long-interval chronochrome target detection," Int. Symp. Spectral Sens. Res., (1997)
[24] Ayhan, B. and Kwan, C., "On the use of Radiance Domain for Burn Scar Detection under Varying Atmospheric Illumination Conditions and Viewing Geometry," Journal of Signal Image and Video Processing, 11, 605–612 (2016).
[25] Zhou, J., Kwan, C., Ayhan, B. and Eismann, M., "A Novel Cluster Kernel RX Algorithm for Anomaly and Change Detection Using Hyperspectral Images," IEEE Trans. Geoscience and Remote Sensing, 54, 6497-6504 (2016).
[26] Kwan, C., Hagen, L., Chou, B., Perez, D., Li, J., Shen, Y. and K. Koperski, "Simple and Efficient Cloud and Shadow Detection Algorithms for Landsat and Worldview images," Journal of Signal, Image, and Video Processing, submitted, (2019).
[27] Zhou, J., Kwan, C. and Budavari, B., "Hyperspectral Image Super-Resolution: A Hybrid Color Mapping Approach," SPIE Journal of Applied Remote Sensing, 10, (2016)
[28] Kwan, C., Budavari, B., Bovik, A.C. and Marchisio, G., "Blind Quality Assessment of Fused WorldView-3 Images by Using the Combinations of Pansharpening and Hypersharpening Paradigms," IEEE Geoscience and Remote Sensing Letters, 14(10), 1835 - 1839 (2017)